Optics Communications 368 (2016) 34–38

Contents lists available at ScienceDirect

Optics Communications

journal homepage: www.elsevier.com/locate/optcom

Focusing properties of phase-only generalized Fibonacci photon sieves

Jie Ke [a,b], Junyong Zhang [a,*]

[a] Shanghai Institute of Optics and Fine Mechanics, Chinese Academy of Sciences, Shanghai 201800, China
[b] University of Chinese Academy of Sciences, Beijing 100049, China

ARTICLE INFO

Article history:
Received 12 August 2015
Received in revised form
8 October 2015
Accepted 26 January 2016
Available online 4 February 2016

Keywords:
Diffractive lenses
Generalized Fibonacci sequence
Photon sieve
Spiral phase
X-ray optics

ABSTRACT

We propose a new algorithm to extend the standard Fibonacci photon sieve to the phase-only generalized Fibonacci photon sieve (GFiPS) and find that the focusing properties of the phase-only GFiPS are only relevant to the characteristic roots of the recursion relation of the generalized Fibonacci sequences. By switching the transparent and opaque zones on the basis of the generalized Fibonacci sequences, we not only realize adjustable bifocal lengths, but also give their corresponding analytic expressions. Besides, we investigate a special phase-only GFiPS, a spiral-phase GFiPS, which can present twin vortices along the axial coordinate. Compared with the single focusing system, bifocal system can be exploited to enhance the processing speed, and offer a broad range of applications, such as direct laser writing, optical tweezers or atom trapping and paralleled fluorescence microscope.

1. Introduction

Focusing of X-ray and extreme ultraviolet (EUV) has many applications in physical and life sciences, such as high-resolution microscopy, spectroscopy, and lithography [1]. A traditional Fresnel zone plate (FZP), which has inherent limitations [2,3], can be used for this kind of focusing [4,5]. Some aperiodic zone plates, generated with the fractal Cantor set, have been proposed to overcome some of these limitations [6,7], another interesting mathematical generator of aperiodic zone plates is the Fibonacci sequence. Photonics is a potential field of applications for novel devices designed and constructed by using a Fibonacci sequence as a consequence of its unique properties. The focusing and imaging properties of Fibonacci optical elements, *e.g.*, quasicrystals [8,9], gratings [10–12], lenses [13–15], zone plates [16], *etc.*, are studied in detail. In mathematics, many mathematicians have extensively studied the Fibonacci sequence and its various generalizations [17,18] in the past decades.

In 2001, Kipp et al. proposed a photon sieve [19], which is a FZP with the transparent zones replaced by a great number of completely separated pinholes to overcome the disadvantages of traditional zone plate. Several kinds of theoretical models [20–22] have been studied mathematically and experimentally [23–26] to design different kinds of photon sieves, such as fractal [27,28], compound [23], Zernike apodized [29], phase zone [30], spiral [31], square [32], and reflection photon sieves [33]. In our previous work, we proposed a bifocal modified Fibonacci photon sieve (MFiPS), designed by using the Fibonacci sequence with two different initial seed elements [34], but the ratio of the two focal lengths is a fixed value.

In this paper, we introduce the aperiodic generalized Fibonacci sequences into photon sieves, and come to a conclusion that the phase-only generalized Fibonacci photon sieve (GFiPS) can generate two equal axial intensity foci with adjustable location. We find the relationship between the focusing properties of a phase-only GFiPS and its characteristic roots of the recursion relation of the generalized Fibonacci sequences. Besides, based on the laser vortex beams generated by use of spiral phase [13,35,36], we present a spiral-phase generalized Fibonacci photon sieve to produce twin vortices along the axial coordinate, which still has the same focusing properties as that mentioned above.

2. Phase-only generalized Fibonacci photon sieves

For the generalized Fibonacci sequences, their initial seed elements are as follows:

$$F_j = a_j \quad (j = 1, 2, 3, a_j \in N^+). \tag{1}$$

And the corresponding linear recursion relation of the generalized Fibonacci sequences can be written as

$$F_n = pF_{n-1} + qF_{n-2} + rF_{n-3} \quad (p, q, r \in R). \tag{2}$$

The absolute value of one of the corresponding characteristic roots of the recursion relation can be defined as the limit of the ratio of two consecutive generalized Fibonacci numbers

* Corresponding author.
E-mail address: zhangjin829@163.com (J. Zhang).

http://dx.doi.org/10.1016/j.optcom.2016.01.075
0030-4018/

$$\gamma = \lim_{j\to\infty} F_j/F_{j-1}. \tag{3}$$

When $(p,\ q,\ r)=(1,\ 1,\ 0)$, we can get the standard Fibonacci sequence. Obviously, $x_1=(1+\sqrt{5})/2$ and $x_2=(1-\sqrt{5})/2$, which are associated with the classical geometrical problem of the golden section, are its characteristic roots of the characteristic equation $x^2-x-1=0$.

We now retrospect the design of a FZP based on the plane wave incidence. All the designed rays are converged upon a single point. As known, the radius of the mth zone can be determined by [4]

$$r_m = \sqrt{(m\lambda/2)^2 + m\lambda f}, \tag{4}$$

where f denotes the expected focal length and λ is the incident wavelength.

A phase-only GFiPS can be generated similar to the process of a traditional photon sieve (TPS) [23] and a modified Fibonacci photon sieve [34]. Taking a generalized Fibonacci sequence into account, whose initial seed elements are $F_1=1$, $F_2=2$ and $F_3=3$ and the recursion relation is $F_n=-F_{n-1}+F_{n-2}-F_{n-3}$, where the minus denotes complement operation. After encoding two seed elements as $(F^1,\ F^2,\ F^3)=(0,\ 01,\ 101)$, the six-order switching sequence F^4 is 010011 while 1 denotes transparent zones and 0 denotes opaque ones. That means the number of total zones is six and three zones are transparent. The corresponding phase-only GFiPS is shown in Fig. 1(b), which is a generalized Fibonacci zone plate (GFiZP) [see Fig. 1(a)] with the transparent and opaque zones replaced by a great number of completely separated pinholes, and their phases are 0 and π, respectively. The diameter d of the pinholes in the mth zone of w in width should take the value of $d=1.16w$ [34].

3. Simulation and discussion

Theoretically, the diffraction field of the phase-only GFiPS can be numerically calculated by the Rayleigh–Sommerfeld diffraction integral formula under the condition of a plane wave incidence with unit amplitude [37–39]

$$U(x,\ y,\ z) = \iint_{\Sigma} t(\xi,\ \eta,\ 0)\frac{\exp(ikR)}{i\lambda R}\left(1+\frac{i}{kR}\right)\frac{z}{R}\mathrm{d}\xi\mathrm{d}\eta, \tag{5}$$

where $t(\xi,\ \eta,\ 0)$ is the pupil function of a GFiPS, i is the imaginary unit, k is the wave number, z is the axial distance from the pupil plane, and R denotes the distance between point $(\xi,\ \eta,\ 0)$ and point $(x,\ y,z)$.

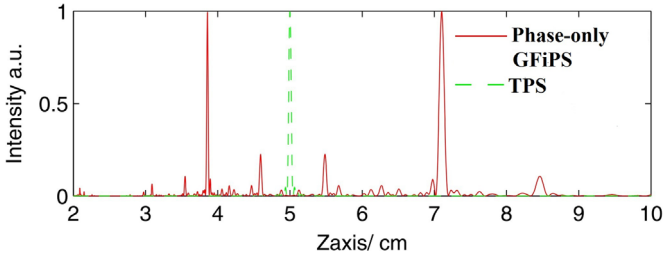

Fig. 2. Normalized intensity distribution along the optical axis produced by a phase-only GFiPS and a TPS with the same resolution.

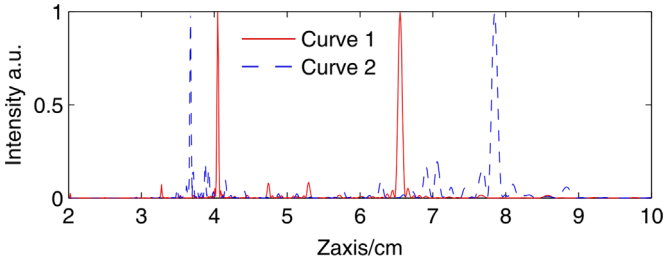

Fig. 3. Normalized axial intensity distribution produced by two phase-only GFiPSs based on different generalized Fibonacci sequences. Curve 1: $F_n=-F_{n-1}+F_{n-2}$ (F^{11} in this case); curve 2: $F_n=2F_{n-1}+0.3F_{n-2}$ (F^8 in this case).

Table 1
The focusing properties of phase-only GFiPSs.

Sequences		**(*p*, *q*, *r*)**		
		(−1,1,−1)	(−1,1,0)	(2,0.3,0)
Total zones		230	233	241
γ		|−1.839|	|−1.618|	2.140
***a* (mm)**		2.716	2.716	2.762
Focal lengths based on Eq. (6)	f_{I} **(cm)**	3.862	4.048	3.670
	f_{II} **(cm)**	7.103	6.549	7.854
Focal lengths based on numerical calculation	f_1 **(cm)**	3.861	4.047	3.675
	f_2 **(cm)**	7.107	6.549	7.849
	f_2/f_1	1.841	1.618	2.136

To investigate the focusing performance of the phase-only GFiPSs, some numerical simulations are done with the incident wavelength λ of 632.8 nm, the expected focal length f of 5 cm. Based on Eq. (5), we use FFT method in the following simulation in HP Z800 workstation.

First of all, a phase-only GFiPS of ten-order switching sequence F^{10} is discussed. Its encoded seed elements are $(F^1,\ F^2,\ F^3)=(0,\ 01,\ 011)$,

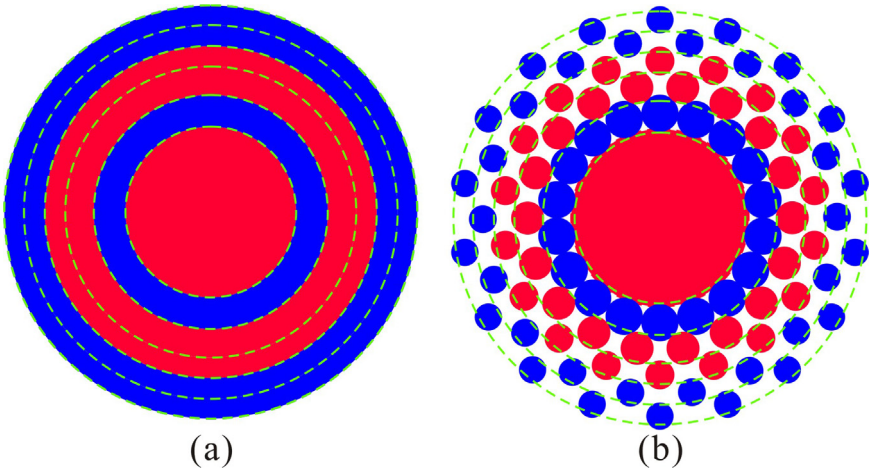

Fig. 1. (a) A generalized Fibonacci zone plate. (b) A phase-only generalized Fibonacci photon sieve.

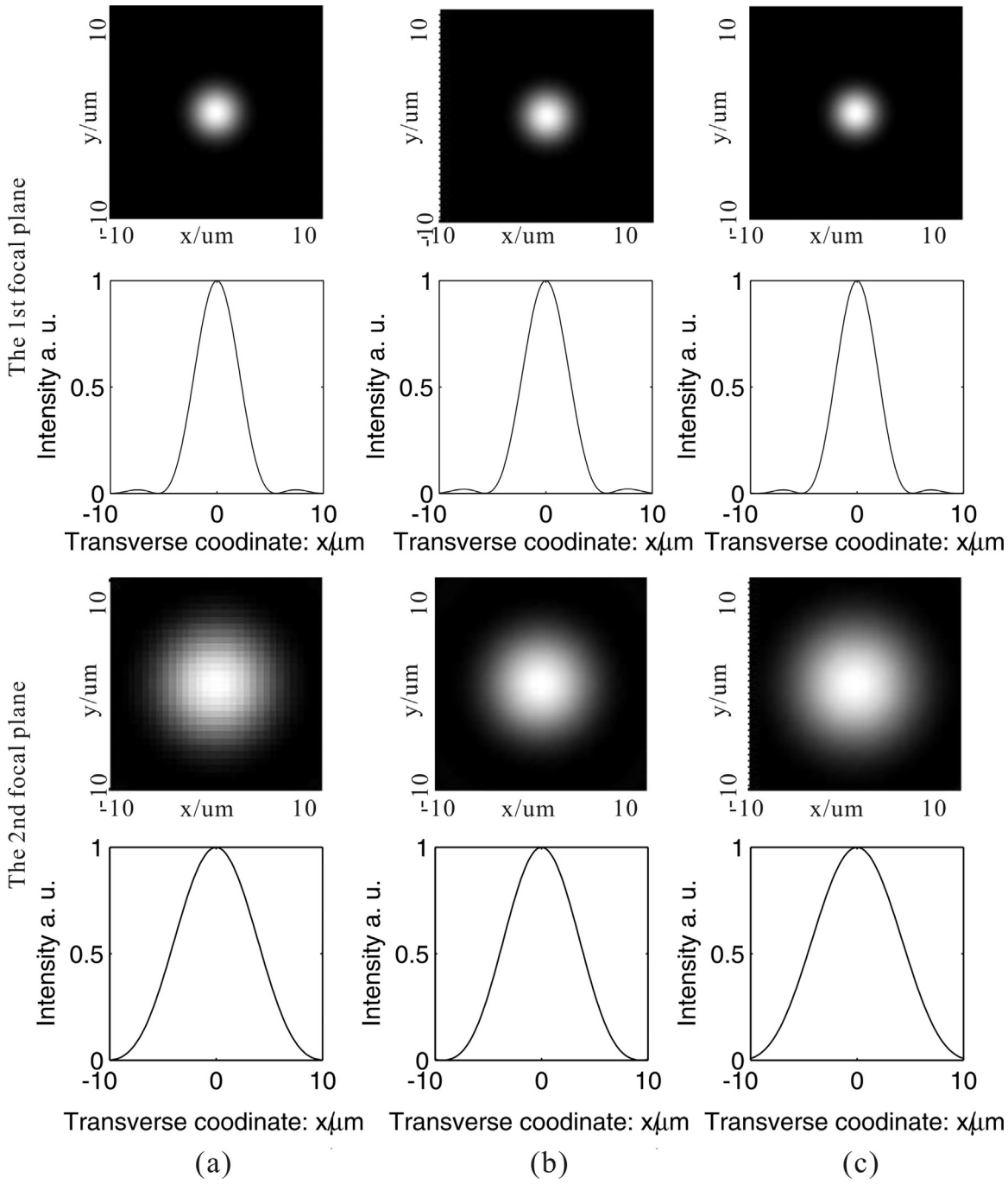

Fig. 4. Normalized transverse intensity distribution produced by three phase-only GFiPSs based on different generalized Fibonacci sequences. (a) $F_n=-F_{n-1}+F_{n-2}-F_{n-3}$ (F^{10} in this case); (b) $F_n=-F_{n-1}+F_{n-2}$ (F^{11} in this case); (c) $F_n=2F_{n-1}+0.3F_{n-2}$ (F^{8} in this case).

and the corresponding linear recursion relation is $F_n=-F_{n-1}+F_{n-2}-F_{n-3}$, whose characteristic equation is $x^3+x^2-x+1=0$, and the characteristic roots are -1.839, $0.420+0.606i$, and $0.420-0.606i$, respectively. For comparison, a TPS with the same resolution is represented. The number of transparent zones is 125 for the phase-only GFiPS and 115 for the TPS while each of them has a total of 230 zones. Their radii are all 2.716 mm. The axial normalized intensity computed for the phase-only GFiPS and the associated TPS are shown in Fig. 2. Obviously, in this case, the first focus of the phase-only GFiPS is located at $f_1=3.856$ cm and the other one at $f_2=7.102$ cm while the prime focal length of TPS is 4.999 cm. Thus, the ratio of the two focal lengths satisfies $f_2/f_1=1.842$, which is approximately equal to the absolute value of one of the corresponding characteristic roots $\gamma=|-1.839|$. Actually it has been indicated that the standard Fibonacci sequence can be regarded as two incommensurable periods [40]. In this case, we can divide the generalized Fibonacci sequences into two periods under the proper encoding. The two lengths are as follows: $N_1=2N/(\gamma^{-1}+1)$ and $N_2=2N/(\gamma+1)$, where N is the total of zones. Hence, the two focal lengths can be expressed as

$$f_{\mathrm{I}}=\frac{a^2}{\lambda N_1}, f_{\mathrm{II}}=\frac{a^2}{\lambda N_2} \tag{6}$$

where a is the radius of a phase-only GFiPS. Theoretically, the two focal lengths should be $f_{\mathrm{I}}=3.862$ cm and $f_{\mathrm{II}}=7.103$ cm, which are agree with the simulation results very well.

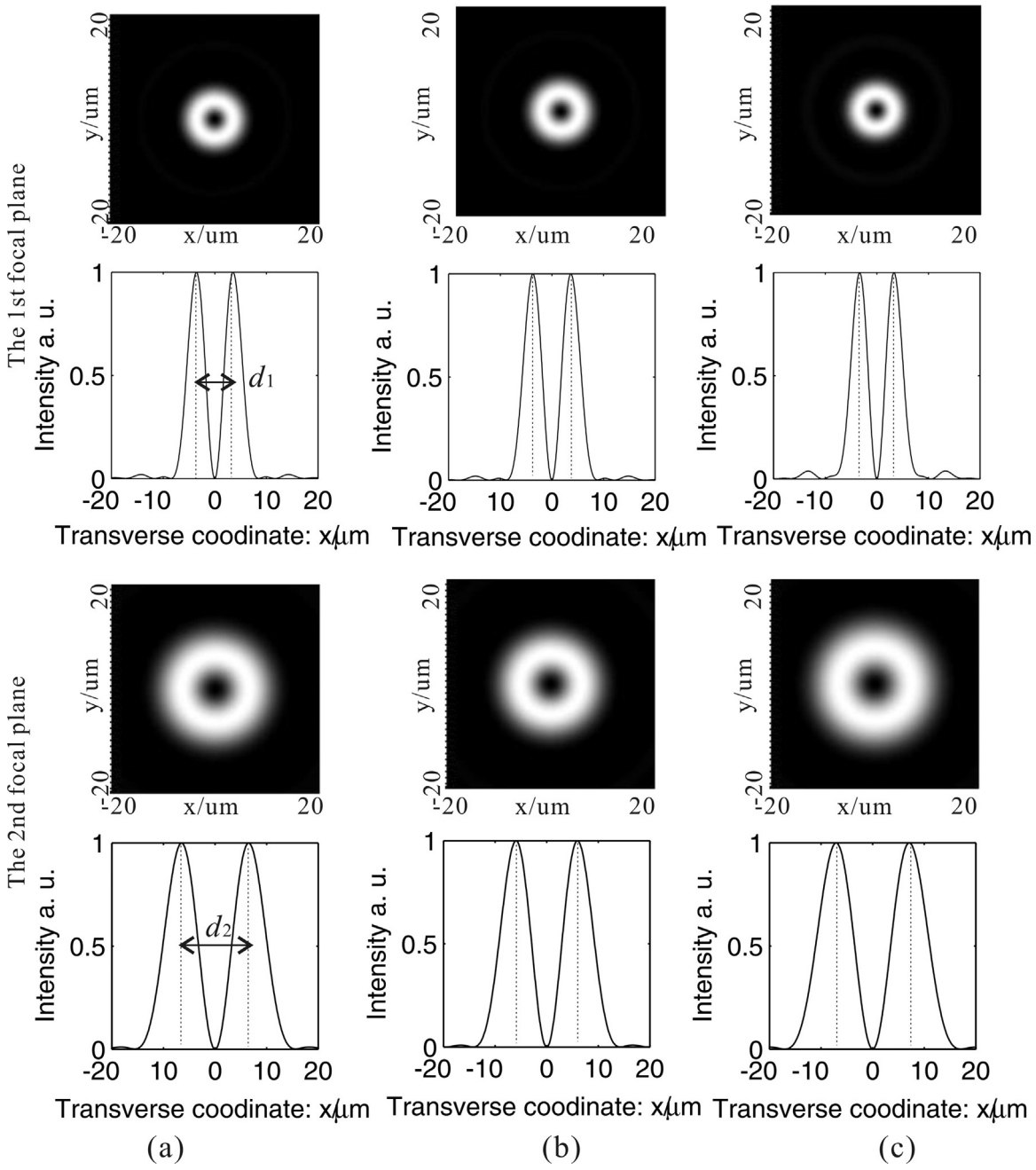

Fig. 5. Normalized transverse intensity distribution produced by three spiral-phase GFiPSs based on different generalized Fibonacci sequences. (a) $F_n=-F_{n-1}+F_{n-2}-F_{n-3}$ (F^{10} in this case); (b) $F_n=-F_{n-1}+F_{n-2}$ (F^{11} in this case); (c) $F_n=2F_{n-1}+0.3F_{n-2}$ (F^{8} in this case).

Table 2
The focusing properties of spiral-phase GFiPSs.

Sequences		**(*p*, *q*, *r*)**		
		(−1,1,−1)	(−1,1,0)	(2,0.3,0)
Total zones		230	233	241
γ		|−1.839|	|−1.618|	2.140
***a* (mm)**		2.716	2.716	2.762
Diameter of the focal rings	d_1 (μm)	3.563	3.616	3.313
	d_2 (μm)	6.479	5.932	7.076
	d_2/d_1	1.818	1.618	2.136

An Fibonacci photon sieve can present two equal intensity foci and the ratio of the two focal lengths approaches the golden mean [34] which is a fixed value. But for a phase-only GFiPS, the ratio may be adjustable due to the different generalized Fibonacci sequences.

For the purpose of adjustable ratio of the two axial focal lengths, the other two kinds of phase-only GFiPSs are investigated. The two generalized Fibonacci sequences are $F_n=-F_{n-1}+F_{n-2}$ and $F_n=2F_{n-1}+0.3F_{n-2}$ and the values γ are $|-1.618|$ and 2.118, respectively. Besides, the encoded seed elements are all $(F^1, F^2)=$ (01, 010). Fig. 3 shows axial intensity distribution produced by phase-only GFiPS. The ratio of the two focal lengths changes from 1.618 to 2.140 due to the different generalized Fibonacci sequences. Table 1 shows the focusing properties of phase-only GFiPSs. It is necessary to point out that the ratio of two focal lengths generated by the generalized Fibonacci sequences with the proper encoding can be equal to γ. More important, it suggests that the ratio of two focal lengths is also adjustable and just relevant to the given

switching sequence. Moreover, it also suggest that the theoretical focal lengths based on Eq. (6) agree well with simulation results. This focusing properties offer an operable instruction for designing bifocal diffraction optical elements conformed to actual requirement.

To further study the transverse focusing properties of the phase-only GFiPS, Fig. 4 shows the intensity maps and the transverse intensity distribution of three aforementioned phase-only GFiPSs at the two focal planes. In Fig. 4(a), the full-width at half-maximum (FWHM) of the two focal spots are $r_1=2.343$ μm and $r_2=4.306$ μm, whose axial focusing distribution was shown in Fig. 3 with solid line. Interestingly, $r_2/r_1=1.838\approx\gamma=|-1.839|$. In other words, the ratio of FWHM of two focal spots is approximately equal to the absolute value of one of its characteristic roots. Other two phase-only GFiPSs also have the similar focusing property. The FWHM of the two focal spots are 2.420 μm and 3.928 μm in Fig. 4(b), and 2.194 μm and 4.650 μm in Fig. 4(c). Furthermore, we can use super-Gaussian amplitude modulation technology to improve the transverse resolution [34].

Laser vortex beams are generated using a spiral phase, which is generally more energy efficient in comparison with other optical elements. So we introduce the spiral phase into a phase-only GFiPS to form a spiral-phase GFiPS, which is a GFiZP with the transparent zones replaced by a great number of completely separated pinholes, and their phases change from 0 to 2π in each zone. Fig. 5(a), (b) and (c) shows the numerically simulated transverse intensity and the intensity maps at the two focal planes for three spiral-phase GFiPSs. From Table 2, we find that the diameters of the focal rings, d, conforms to the rule *i.e.* $d_2/d_1\approx\gamma$. Hence, the spiral-phase GFiPSs can generate twin axial vortices.

4. Summary

In conclusion, we proposed a new family of photon sieves which can be designed based on the generalized Fibonacci sequences, and investigated the axial and transverse focusing properties of the phase-only GFiPS. It suggested that phase-only GFiPSs presented two axial foci with equal intensity. We found the relationship between focusing properties of the phase-only GFiPSs and their characteristic roots, and gave the analytic expressions of the corresponding focal lengths. But for spiral-phase GFiPSs, they can produce a twin optical vortices along the axial coordinate. We believe that the phase-only GFiPSs and the spiral-phase GFiPSs may offer a broad range of applications, such as direct laser writing, optical tweezers or atom trapping and paralleled fluorescence microscope.

Acknowledgments

This work was supported by the National Natural Science Foundation of China (Nos. 61205212 and 61205210).

References

[1] B. Yu, W. Jia, C. Zhou, H. Cao, W. Sun, Grating imaging scanning lithography, Chin. Opt. Lett. 11 (2013) 080501.
[2] H. Kyuragi, T. Urisu, Higher-order suppressed phase zone plates, Appl. Opt. 24 (1985) 1139–1141.
[3] J.A. Sun, A. Cai, Archaic focusing properties of Fresnel zone plates, J. Opt. Soc. Am. A 8 (1991) 33–35.
[4] J. Kirz, Phase zone plates for X rays and the extreme UV, J. Opt. Soc. Am. 64 (1974) 301–309.
[5] E.H. Adnderson, V. Boegli, L.P. Muray, Electron beam lithography digital pattern generator and electronics for generalized curvilinear structures, J. Vac. Sci. Techol. B 13 (1995) 2529–2534.
[6] G. Saavedra, W.D. Furlan, J.A. Monsoriu, Fractal zone plates, Opt. Lett. 28 (2003) 971–973.
[7] J.A. Davis, S.P. Sigarlaki, J.M. Craven, M.L. Calvo, Fourier series analysis of fractal lenses: theory and experiments with a liquid-crystal display, Appl. Opt. 45 (2006) 1187–1192.
[8] L.D. Negro, C.J. Oton, Z. Gaburro, L. Pavesi, P. Johnson, A. Lagendijk, R. Righini, M. Colocci, D.S. Wiersma, Light transport through the band-edge states of fibonacci quasicrystals, Phys. Rev. Lett. 90 (2003) 055501.
[9] M. Verbin, O. Zilberberg, Y. Lahini, Y.E. Kraus, Y. Silberberg, Topological pumping over a photonic Fibonacci quasicrystal, Phys. Rev. B 91 (2015) 064201.
[10] N. Gao, Y. Zhang, C. Xie, Circular Fibonacci gratings, Appl. Opt. 50 (2011) G142–G148.
[11] R. Verma, V. Banerjee, P. Senthilkumaran, Fractal signatures in the aperiodic Fibonacci grating, Opt. Lett. 39 (2014) 2257–2260.
[12] R. Verma, M.K. Sharma, P. Senthilkumaran, V. Banerjee, Analysis of Fibonacci gratings and their diffraction patterns, J. Opt. Soc. Am. A 31 (2014) 1473–1480.
[13] A. Calatayud, V. Ferrando, L. Remon, W.D. Furlan, J.A. Monsoriu, Twin axial vortices generated by Fibonacci lenses, Opt. Express 21 (2013) 10234–10239.
[14] J.A. Monsoriu, A. Calatayud, L. Remon, W.D. Furlan, G. Saavedra, P. Andres, Bifocal Fibonacci diffractive lenses, IEEE Photonics J. 5 (2013) 3400106.
[15] V. Ferrando, A. Calatayud, P. Andres, R. Torroba, W.D. Furlan, J.A. Monsoriu, Imaging Properties of kinoform Fibonacci lenses, IEEE Photonics J. 6 (2014) 6500106.
[16] H.T. Dai, Y.J. Liu, X.W. Sun, The focusing property of the spiral Fibonacci zone plate, Proc. SPIE 8257 (2012) 82570T.
[17] D.A. Wolfram, Solving generalized Fibonacci recurrences, Fibonacci Q. 36 (1998) 129–145.
[18] A. Wloch, Some identities for the generalized Fibonacci numbers and the generalized Lucas numbers, Appl. Math. Comput. 219 (2013) 5564–5568.
[19] L. Kipp, M. Skibowski, R.L. Johnson, R. Berndt, R. Adelung, S. Harm, R. Seemann, Sharper images by focusing soft X-rays with photon sieves, Nature 414 (2001) 184–187.
[20] Q. Cao, J. Jahns, Focusing analysis of the pinhole photon sieve: individual far field model, J. Opt. Soc. Am. A 19 (2002) 2387–2393.
[21] Q. Cao, J. Jahns, Nonparaxial model for the focusing of highnumerical-aperture photon sieves, J. Opt. Soc. Am. A 20 (2003) 1005–1012.
[22] J. Zhang, Q. Cao, X. Lu, Z. Lin, Focusing contribution of individual pinholes of a photon sieve dependence on the order of local ring of underlying traditional Fresnel zone plate, Chin. Opt. Lett. 8 (2010) 256–258.
[23] C. Zhou, X. Dong, L. Shi, C. Wang, C. Du, Experimental study of a multi-wavelength photon sieve designed by random-area-divided approach, Appl. Opt. 48 (2009) 1619–1623.
[24] J.M. Davila, High-resolution solar imaging with a photon sieve, Proc. SPIE 8148 (2011) 81480O.
[25] R. Menon, D. Gil, G. Barbastathis, H.I. Smith, Photon-sieve lithography, J. Opt. Soc. Am. A 22 (2005) 342–345.
[26] G. Andersen, Large optical photon sieve, Opt. Lett. 30 (2005) 2976–2978.
[27] F. Giménez, J.A. Monsoriu, W.D.F.A.A. Pons, Fractal photon sieve, Opt. Express 14 (2006) 11958–11963.
[28] F. Gimenez, W.D. Furlan, J.A. Monsoriu, Lacunar fractal photon sieves, Opt. Commun. 277 (2007) 1–4.
[29] G. Cheng, C. Hu, P. Xu, T. Xing, Zernike apodized photon sieves for high-resolution phase-contrast X-ray microscopy, Opt. Lett. 35 (2010) 3610–3612.
[30] J. Jia, C. Xie, Phase zone photon sieve, Chin. Phys. B 18 (2009) 183–188.
[31] C. Xie, X. Zhu, L. Shi, M. Liu, Spiral photon sieves apodized by digital prolate spheroidal window for the generation of hard-X-ray vortex, Opt. Lett. 31 (2010) 1765–1767.
[32] J. Zhang, Q. Cao, X. Lu, Z. Lin, Individual far-field model for photon sieves composed of square pinholes, J. Opt. Soc. Am. A 27 (2010) 1342–1346.
[33] M. Kalläne, J. Buck, S. Harm, R. Seemann, K. Rossnagel, L. Kipp, Focusing light with a reflection photon sieve, Opt. Lett. 36 (2011) 2405–2407.
[34] J. Ke, J. Zhang, J. Zhu, Focusing properties of a modified Fibonacci photon sieve, Chin. Opt. Lett. 13 (2015) 080501.
[35] A. Sakdinawat, Y. Liu, Soft-X-ray microscopy using spiral zone plates, Opt. Lett. 32 (2007) 2635–2637.
[36] B. Zhang, D. Zhao, Focusing properties of Fresnel zone plates with spiral phase, Opt. Express 18 (2010) 12818–12823.
[37] J.E. Harvey, Fourier treatment of near-field scalar diffraction theory, Am. J. Phys. 47 (1979) 974–980.
[38] W.H. Southwell, Validity of the Fresnel approximation in the near field, J. Opt. Soc. Am. 71 (1981) 7–14.
[39] C.J.R. Sheppard, M. Hrynevych, Diffraction by a circular aperture: a generalization of Fresnel diffraction theory, J. Opt. Soc. Am. A 9 (1992) 274–281.
[40] E. Macia, Exploiting aperiodic designs in nanophotonic devices, Rep. Prog. Phys. 75 (2012) 036502.